Magnetic Properties of Hybrid Inorganic-organic Flexible Nanofibers

Omar A. Hussein[1*], T.H. Mubarak[2], Isam M. Ibrahim[3]

Abstract

Polypyrrole nanofibers (PPy-NFs) had prepared via chemical oxidation of pyrrole monomer by Iron (III) chloride in the presence of methyl orange. As well as, Nanomagnetic particles of $Co_{0.8}Mn_{0.2}Fe_2O_4$ and $Zn_{0.8}Mn_{0.2}Fe_2O_4$ had synthesized by the hydrothermal autoclave reactor after use co-precipitation technique. The PPy-NFs nanocomposite that obtained from decorating of PPy-NFs with Nanomagnetic particles. The XRD studied showed that the (PPy-NFs) is non-crystalline and the average crystallite size of $Co_{0.8}Mn_{0.2}Fe_2O_4$ and $Zn_{0.8}Mn_{0.2}Fe_2O_4$ were 8.54 and 14.47 nm respectively. These two belong to single phase cubic spinel. FESEM studies exhibit that PPy has a nanofibers structure with distinct diameters and most the magnetic nanoparticles had homogeneous distribution and had sphere form. The saturation magnetization (M_s) increased with increasing ferrite content in the nanocomposite samples, according to magnetic hysteresis loop measurements. As its increases in pure ferrite samples by increases cobalt ions. The M_s Values of $Co_{0.8}Mn_{0.2}Fe_2O_4$, $Zn_{0.8}Mn_{0.2}Fe_2O_4$ and PPy-NFs were 41.15 emu/g, 10.13 emu/g and 14.95 emu/g respectively.

Key Words: PPy-NFs, Hysteresis Loop, Nanomagnetic, Spinel Ferrite.

DOI Number: 10.14704/nq.2022.20.4.NQ22096 **NeuroQuantology 2022; 20(4):64-72**

Introduction

Conductive polymer composites with ferromagnetic and electrical characteristics had recently become very famous study subjects. The creation of composites containing magnetic nanoparticles (NPs) inserted in a conductive polymer matrix, such as polyaniline and polypyrrole, with all-in-one optical, magnetic, electrical capabilities has attracted attention (Ahuja & Kumar, 2009; Cabrera, Gutierrez, Morales, Menendez, & Herrasti, 2009; De, Sen, Poddar, & Das, 2009).

The creation of nanoparticles wrapped with polymer layers allowed for much more domain and forming of magnetic nanoparticles. Hybrid organic-inorganic nanocomposites with improved optical, electrochemical, magnetic features and thermal stability are created by encapsulating metal nanoparticles into Conducting polymers or vice versa, as in our study. Furthermore, the size and shape of the particles in such polymer-coated metal composite materials have a significant impact on their characteristics (Choi & Jang, 2008; Reddy, Lee, Lee, & Gopalan, 2008).

Due to its unique characteristics and exceptional environmental durability, polypyrrole (PPy) is one of the most promising conducting polymers (Zhang, Li, & Ye, 2009). In the last three decades, conducting polymers have evolved as a new class of materials. Potential applications such as microwave absorbers were carefully examined soon after these materials were discovered because of their high conductivity, fascinating electrical characteristics, and ease of manufacture (Truong, Riddell, & Muscat, 1998).

Corresponding author: Omar A. Hussein
Address: [1*]Department of Physics, College of Science, University of Diyala, Diyala, Iraq; [2]Department of Physics, College of Science, University of Diyala, Diyala, Iraq; [3]Department of Physics, College of Science, University of Baghdad, Baghdad, Iraq.
E-mail: [1*]omarah10@yahoo.com, [2]dean@sciences.uodiyala.edu.iq, [3]dr.issamiq@gmail.com
Relevant conflicts of interest/financial disclosures: The authors declare that the research was conducted in the absence of any commercial or financial relationships that could be construed as a potential conflict of interest.
Received: 30 January 2022 **Accepted:** 12 March 2022

Conducting polymers can efficiently shield electromagnetic waves generated from an electric source, but magnetic materials can only effectively shield electromagnetic waves generated by a magnetic source. As a result, incorporating magnetic components and conducting polymeric materials into multifunctional composites opens up new opportunities for achieving good shielding effectiveness for a variety of electromagnetic sources (Birsöz, Baykal, Sözeri, & Toprak, 2010).

Ferrites are widely used in many fields of telecommunications and electronics engineering, and they come in a wide range of compositions, features, and applications. Fine ferrites, which are comprised of iron oxides, manganese, zinc, and cobalt, have been of particular interest due to their uses in a variety of industries. This ferrite belongs to the soft ferrite family, which is distinguished by high magnetic permeability and low losses. These materials are widely employed in microwave devices, magnetic recording media, computer memory chips, transformer cores, radio frequency coil manufacturing and rod antennas, among other applications (Abbas, Khan, Ahmad, & Anwar, 1992; Ghazanfar, Siddiqi, & Abbas, 2005).

In light of the foregoing, the purpose of this paper is to present the synthesis and characterization of the magnetic behavior of polypyrrole modified with small amounts of nanoferrite species, as it is currently very appealing to discover a magnetic semiconductor at room temperature whose properties can be easily controlled by preparation variables.

Experimental Work

Synthesis of PPy Nanofibers (PPy-NFs)

By chemical polymerization method, 2.5 mM (0.08185 g) methyl orange (MO) (LTD Rubilabor Chemical Co. Spain) was dissolved in de-ionized water (288 ml) and mixed with (14 mM) pyrrole monomer (Sigma Aldrich, China) to form a (Pyrrole monomer-methyl orange) solution that was refrigerated to 3^0C by ice bath. The mixture was stirred well until completely dissolved and agglomerates disappeared for 10 minutes. 1.702 (10mM) ($FeCl_3$) (AlPHA chemica) is dissolved in (33 ml) de-ionized water (see table 1). Then, added drop-wise during 2 hour into (Py-MO) solution. Thereafter, all the above reaction solutions were stirred for one day (24 hour) in an ice bath. The precipitated of PPy-NFs had isolated by filtration and rinsing by acetone, alcohol and water 3 times each stage to isolate the remaining impurities in PPy-NFs. Lastly, the substance was dried by oven at 75°C for six hours.

Table 1. Shows the molar ratio of (PPy-NFs) samples

Sample	MO		Py		$FeCl_3$		MO: Py: $FeCl_3$ Molar ratio
	Weight (g)	No. mol (mM)	Weight (g)	No. mol (mM)	Weight (g)	No. mol (mM)	
PPy-NFs	0.0180	2.5	0.987	14	1.703	10	1: 5.6: 4

Synthesis of Ferrite Nanoparticles

Synthesis of ferrite nanoparticles ($Zn_{0.8}Mn_{0.2}Fe_2O_4$ and $Co_{0.8}Mn_{0.2}Fe_2O_4$) was performed by the co-precipitation technology, combined with the hydrothermal synthesis. This method is summarized as the following steps; we dissolve a stoichiometric amounts of $FeCl_3$ (8.1105g, 50 mM), $MnCl_2.4H_2O$ (0.9895g, 5 mM) (AlPHA chemical), $CoCl_2$ (2.5968g, 20 mM) (AlPHA chemical) and $ZnCl_2$ (2.7257g, 20 mM) (ROMIL pure chemistry) in deionized water in independent beakers (see table 2). Then, they have been moved to another heat-resistant beaker with unbroken stirring to gain a uniform solution. As, in 100ml deionized water, sodium hydroxide (NaOH, 1.25 ML^{-1}) (ROMIL pure chemistry) was dissolved separately. Then it was dropped in metal salt solution at 27°C until the pH reached 12, to make sure that metal ions are precipitated. After 60 min of heating at 90°C with constant stirring, the solution was turned off and permitted to cool at 27°C. The magnetic decantation process was used to separate and collect ferrite nanoparticles. Then, it had washed with deionized water for several times by using a multi-funnels system. In NaOH solution (pH of 12), the moisture outcome has re-dispersed by stirring for 60 minutes. The heat treatment, which was done using the hydrothermal method, was the following step in the fabrication process. The colloidal solution was transferred to a 250 ml Teflon-lined autoclave reactor. After closing the autoclave tightly, it was positioned in a furnace at

250°C for 5h. after a while, it let cool outdoor naturally at 27⁰C. Then, the colloidal solution is filtered and washed with ethanol and deionized water several times for each one until PH even to 7. The material precipitate is ultimately place in the oven at 70°C for 60 min to gain a stable phase of nanoferrite material.

Table 2. Shows the weights utilized in the synthesis of ($Co_{0.8-x}Zn_xMn_{0.2}Fe_2O_4$) from basic chemical compounds.

x	Structure	$FeCl_3$		$MnCl_2.H_2O$		$CoCl_2$		$ZnCl_2$	
		Wight (g)	No. mol (mM)	Wight (g)	No. mol (mM)	Wight (g)	No. mol (mM)	Wight (g)	No. mol (mM)
0	$Co_{0.8}Mn_{0.2}Fe_2O_4$	8.1105	50	0.9895	5	2.5968	20	0	0
0.8	$Zn_{0.8}Mn_{0.2}Fe_2O_4$	8.1105	50	0.9895	5	0	0	2.7257	20

Preparation of PPy-NFs nanocomposite

(3×10^{-2}g) of nanoferrite powder was dissolved in (30 ml) of deionized water was sonicated for ten hours and (3×10^{-2}g) of NFs-PPy was dissolved in 30 ml of distilled water was sonicated for two hours. Then, $Zn_{0.8}Mn_{0.2}Fe_2O_4$ and $Zn_{0.8}Mn_{0.2}Fe_2O_4$ solutions had added to PPy-NFs solution in volumetric proportions. The resulting solution had sonicated for ten hour to get a homogeneous dispersion.

Results and Discussion

X-ray Diffraction Measurements

X-ray diffractometer (XRD 6000-Shimadzu, Japan) working at 40 kV and 30 mA with Cu K (λ =1.5406), scan range: (10º-80º) had used to analyze crystal structures and characterize phase contents for PPy-NFs and nanomagnetic particles.

Figure 1 shows XRD patterns of PPy-NFs. The PPy-NFs powder is amorphous in nature that is non-crystalline solid where the distribution of atoms does not follow any crystalline system. The wide peak had resulted from dissipating X-rays from the chain of the PPy-NFs. In Figure 1 broad peak was observed at about 2θ = 24.5° which are assigned to the (102) directions (Sanches et al., 2015). The broad peak is characteristic of amorphous PPy. A broad halo pattern at ranges 2θ = 10°- 35° is related to PPy-NFs that structured by the oxidative polymerization method and it is typical for doped structure of polypyrrole (MA, SG, PR, Shashwati, & VB, 2011; Ong, Ray, Cooney, Edmonds, & Easteal, 2008). According to the equation (1) that calculated the average chain separation which found to be 4.53Å for PPy-NFs.

$$S = \frac{5\lambda}{8\sin\theta} \qquad (1)$$

Where S is the polymer chain separation, λ is the X-ray wavelength and θ is the diffraction angle at the maximum intensity of the amorphous Halo (Cheah, Forsyth, & Truong, 1998; Ouyang & Li, 1997).

The experimental lattice parameter a_{exp} had calculated according to the following equation:

$$a_{exp} = d\sqrt{h^2 + k^2 + l^2} \qquad (2)$$

Where d is the interplanar distance of each plane and (hkl) are Miller indices. The average crystallite size D_{ave} had calculated by the following well-known Scherrer equation:

$$D_{ave} = K\lambda/\beta\cos\theta \qquad (3)$$

Where D_{ave} is the average crystallite size, K is the Scherrer constant (K =0.94), λ is the wavelength of X-ray used, β is the full width at half maximum and θ is the Bragg angle. The cubic structure of the unit cell volume via equation (4) and The X-ray density d_x were calculated from XRD data by using equation (5).

$$V_c = a_{exp}^3 \qquad (4)$$

$$d_x = \frac{Z\,M}{N_A\,V_c} \qquad (5)$$

Where Z is the number of formula units in a unit cell (Z = 8 for spinel system), M is the molecular weight of the sample, N_A is the Avogadro number and V_c refers to the volume of the cell (Syue, Wei, Chou, & Fu, 2011).

The hopping lengths $L_{A\text{-}A}$, $L_{B\text{-}B}$ and $L_{A\text{-}B}$ between the magnetic ions at the *A*-site and *B*-sites were estimated by the relations (Naseri & Saion, 2012):

$$L_{A-A} = (a_{exp}\sqrt{3})/4 \qquad (6)$$

$$L_{B-B} = (a_{exp}\sqrt{2})/4 \qquad (7)$$

$$L_{A-B} = (a_{exp}\sqrt{11})/8 \qquad (8)$$

Where $L_{A\text{-}A}$, $L_{B\text{-}B}$ and $L_{A\text{-}B}$ are distances Tetra-tetra A-A, Octa-octa B-B, and Tetra-octa A-B, respectively.

Figure 2 shows the XRD analysis of ($Co_{0.8}Mn_{0.2}Fe_2O_4$) compound, a thorough investigation of all cell parameters had conducted. The samples show single phase cubic spinel with Fd3m space group and preferential orientations along (111), (220), (311), (400), (422), (511), (440) and (533). They are indexed with (JCPDs card no. 22-1086). As well as the broadening in the peaks reflects the nanocrystalline nature of these ferrites.

As for the compound ($Zn_{0.8}Mn_{0.2}Fe_2O_4$) in figure 2, The XRD had recorded for 2θ values in the range 10-80 degrees. Where the major peaks obtained (111), (220), (311), (222), (400), (422), (511), (440) and (533). They had indexed well by using JCPDS # (74-2402), ICSD (01-074-2399) and Mn_3O_4 card No. (024-0734). The sample shows expected cubic spinel peaks (Space group: Fd3m) and presence a single-phase structure for ($Zn_{0.8}Mn_{0.2}Fe_2O_4$). As well It can conclude that $Mn^{2+}$and Zn^{2+} ions had well-replaced in the structure of ferrite. However, the analysis of phase assured the existence of Mn_3O_4 in the structure and the width of peaks confirms nanosize particles.

Structural formula of ($Co_{0.8-x}Zn_xMn_{0.2}Fe_2O_4$) is spinel ferrite where the bivalent ions had distributed on both tetrahedral and octahedral sites (Smith & Wijn, 1959). The distribution of cations and structural parameters is strongly based on the preparing method and annealing heat(Kumar, Kumar, Narayan, & Kar, 2013).

The experimental lattice constant (a_{exp}) calculated for highest intensity peak (311) from x-ray diffraction data by using eq. (2) and it inserted in table 3. It is evident that the decline in the lattice parameter occurred because of the substitute of zinc ions with cobalt ions in the tetrahedral site because of Zn^{2+} ions had a tiny ionic radius than Co^{2+} ions.

The crystallite size (D) was estimated from Scherer's eq. (3). It calculated for the strongest reflection at the (311) plane. The highest intensity at the plane (311) arises due to X-rays diffraction from cations that situated at A and B sites (Cullity, 1956). The enhancement of crystallite size has been observed with greater ionic radius Because of the substitution of Zn^{2+} with Co^{2+} in the ferrite structure. Likewise, can perceive that there is effect of zinc substitution on crystallite size because of the crystallite sizes are greatly influenced by the electronic configuration, cation distribution, binding energies and their ionic radius.

X-Ray density is proportional to the molecular weight and the volume of unit cell. It is inversely proportional to the cubic unit cell. X-Ray density calculated from x-ray data by using eq. (5). Molecular mass for the samples that increasing substituted ion (zinc) is greater than cobalt, moreover there is a decrease in the lattice constant by zinc addition. So the zinc increases lead to increases in the density.

The space between two magnetic ions is measured in hopping length (L). such as tetra-tetra A-A (A), octa-octa B-B [B], and tetra-octa A-B. It calculated by using the equations (6, 7 and 8) respectively. From table 3 can be observed that the distances between cations (A-A), (A-B), and (B-B) for the ferrite system reduce with a rise in the Zn concentration. It can be implicit by the truth that an element with greater ionic radius Co^{2+} is substitute by an ionic with lesser ionic radius Zn^{2+}.

Lattice constant (Å), X-ray density, Molecular mass, average crystallite size and hopping lengths for $Co_{0.8-x}Zn_xMn_{0.2}Fe_2O_4$ ferrite are presented in Table 3.

Table 3. XRD data of $Co_{0.8-x}Zn_xMn_{0.2}Fe_2O_4$ nanoparticles

(x)	Lattice constant	X-ray density	Molecular mass	The size of crystallite	Hopping length (Å)		
	$a_{exp(Å)}$	$\rho_{x(\frac{g}{cm^3})}$	g/mol	D_{311}(nm)	L_{A-A}	L_{B-B}	L_{A-B}
0.0	8.45	5.147	233.82	14.47	3.658	2.987	3.503
0.8	8.38	5.393	238.98	8.54	3.628	2.962	3.474

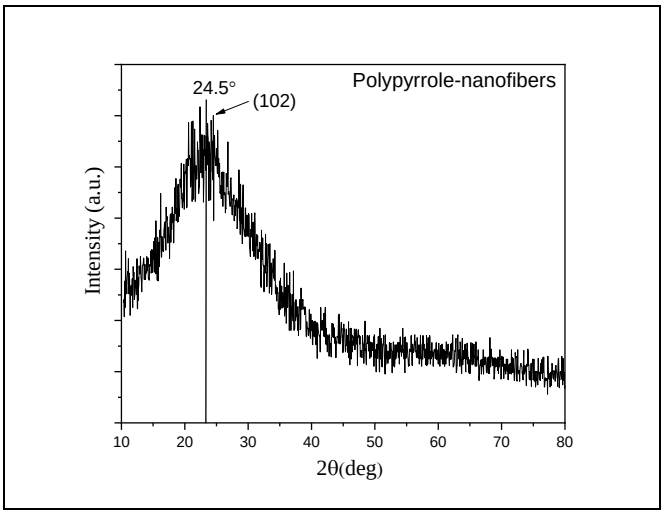

Figure 1. Shows the XRD pattern of (PPy-NFs)

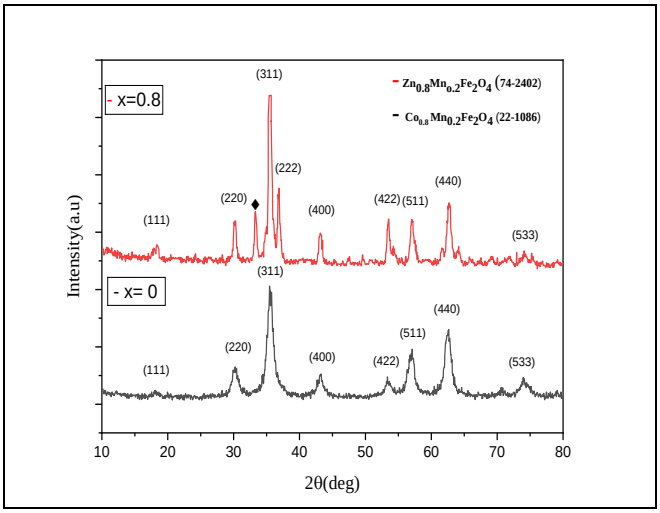

Figure 2. XRD pattern of the $Co_{0.8}Mn_{0.2}Fe_2O_4$ and $Zn_{0.8}Mn_{0.2}Fe_2O_4$ nanoparticles

FESEM Image Analysis

FE-SEM reveals topographical and morphological properties of the composites and pure materials. FESEM images of polypyrrole nanofibers (PPy-NFs) polymer samples synthesized by using chemical oxidative polymerization technique are shown in figure 3. It is observed that all the sample present one dimensional nanofibers, the nanofibers appear having rough surface and vary diameters, with tens of microns in length and diameter between ≈ (50 and 130) nm. The micrograph clearly shows a typical FESEM image of doped PPy-NFs, in addition to the fact that nanostructures are made up of a network of densely entangled twisted and coarse nanofibers.

FESEM images in figure 4 and figure 5 for ferrite nanoparticles ($Co_{0.8}$ $Mn_{0.2}Fe_2O_4$ and $Zn_{0.8}Mn_{0.2}Fe_2O_4$) showing a densed view of the powder sample and homogeneous of grains distribution mostly. Also, the magnetic particles were closely packed and harmonic in the arrangement. These micrographs show nearly spherical particles with the size distributed in a range of ≈ (35-55 nm) and (13-20 nm) for $Co_{0.8}$ $Mn_{0.2}Fe_2O_4$ and $Zn_{0.8}Mn_{0.2}Fe_2O_4$ respectively. As a result, the surface morphological and microstructure images show good agreement with the XRD results. In both samples, only a few pores were found among the particles in the samples. Because of their magnetic characteristics, the magnetic nanoparticles tended to agglomeration together. Furthermore, particles agglomeration together due to emerging forces such as capillary, electrostatic, and Van-der-Wall forces, which cause mutual contacts between nanoparticles.

The decoration of PPy-NFs nanocomposites (PPy-NFs/$Zn_{0.8}Mn_{0.2}Fe_2O_4$ and PPy-NFs/ $Co_{0.8}Mn_{0.2}Fe_2O_4$) had fabricated like a grainy surface structure. It had detected by FE-SEM. From figure 6 and figure 7 the FE-SEM images show that the samples contain both nanoferrites stacked on the PPy-nanofibers surface. Therefore, the figures reveal a gradual rise in ferrite on polymer fibers and enhancement in the attachment of ferrite particles. The magnetic particles are distributed uniformly on the conductive polymer matrix. This indicated that the composites had successfully mixed and blended homogeneously. The ferrite concentration seems useful in occupation the polymer porous sites, increase the interaction surface area and Surface energy. All of these lead to improvement of various structural and electrical properties. Thus, a change would occur in the physical properties such as the shape, size, appearance and state of the material without affecting the internal structure. As, the fibers roughness has a significant impact on the strength of adhesion between the particle and the fiber. Histograms represent diameters distribution of PPy-NFs, $Co_{0.8}Mn_{0.2}Fe_2O_4$ and $Zn_{0.8}Mn_{0.2}Fe_2O_4$ nanoparticles that calculated by Image J software. It confirmed a well agreement with FE-SEM test that shown in figure 8.

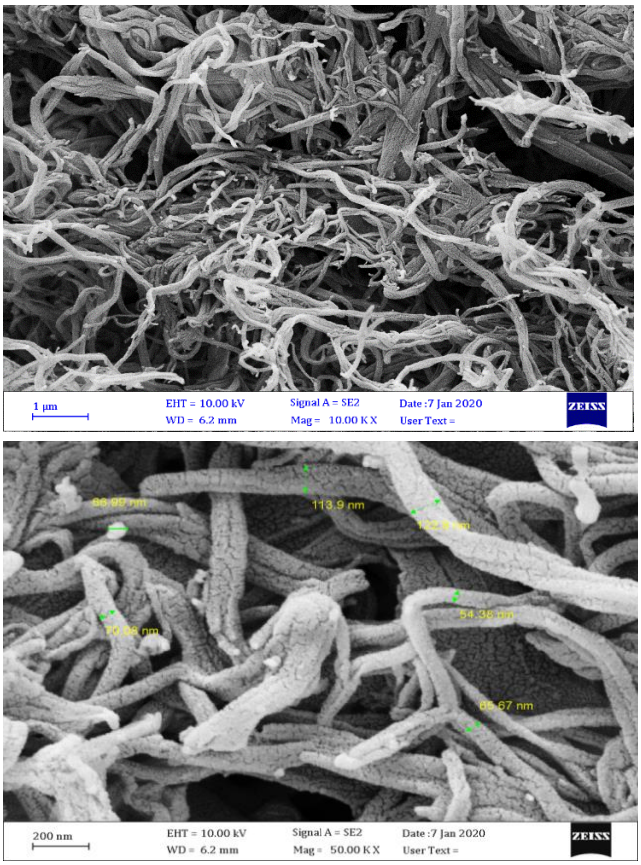

Figure 3. FESEM images of PPy-NFs at different magnification

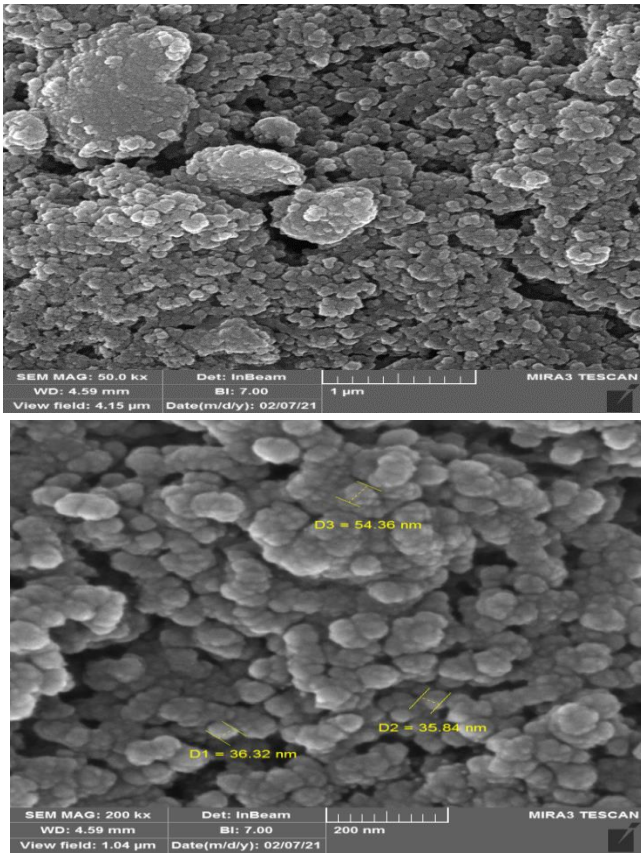

Figure 4. FESEM images of $Co_{0.8}Mn_{0.2}Fe_2O_4$ nanoparticles at different magnification

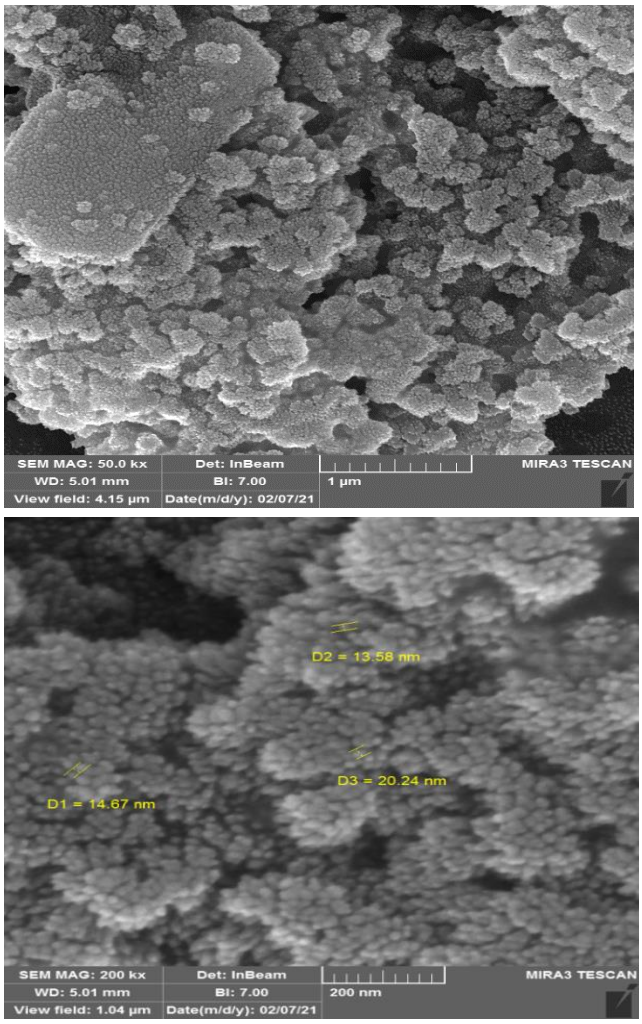

Figure 5. FESEM images of $Zn_{0.8}Mn_{0.2}Fe_2O_4$ nanoparticles at different magnification

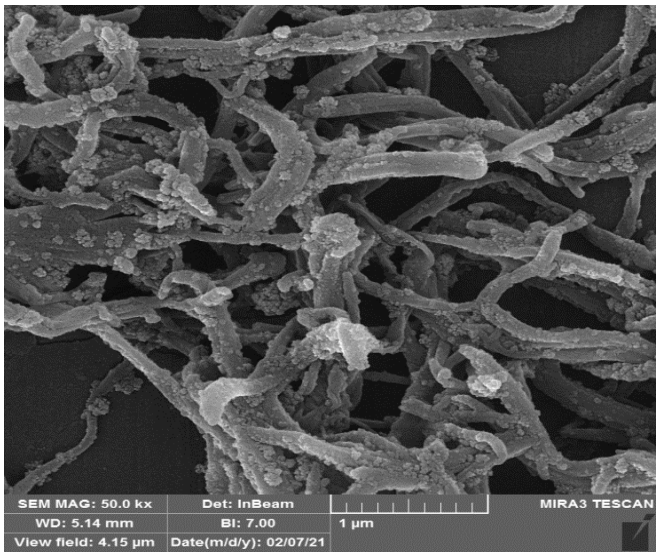

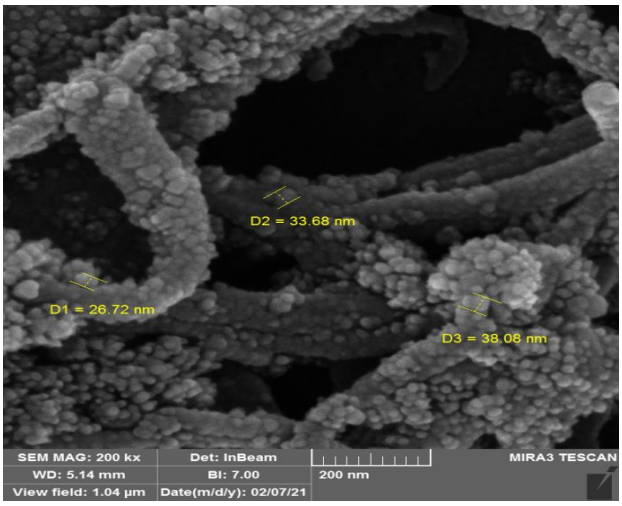

Figure 6. FESEM images of (PPy-NFs/$Co_{0.8}Mn_{0.2}Fe_2O_4$) nanocomposite at different magnification

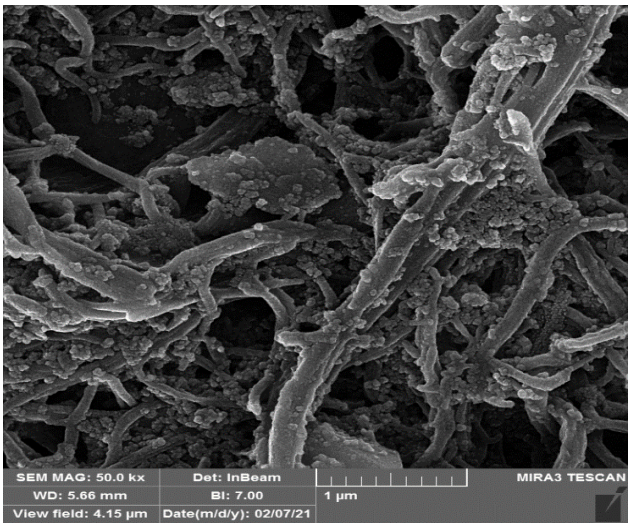

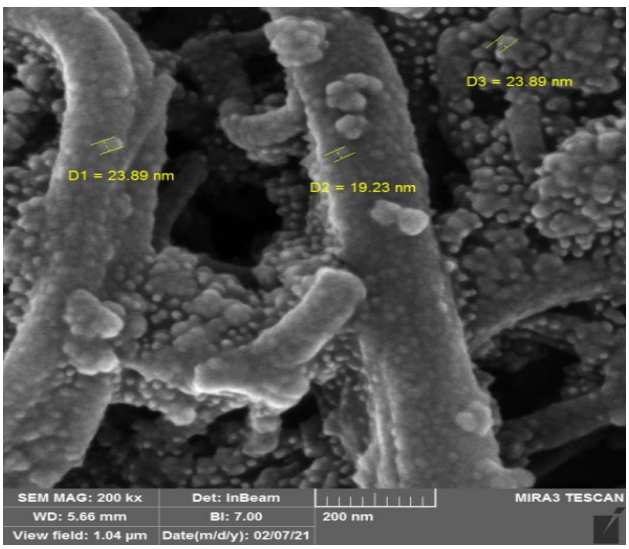

Figure 7. FESEM images of (PPy-NFs/$Zn_{0.8}Mn_{0.2}Fe_2O_4$) nanocomposite at different magnification

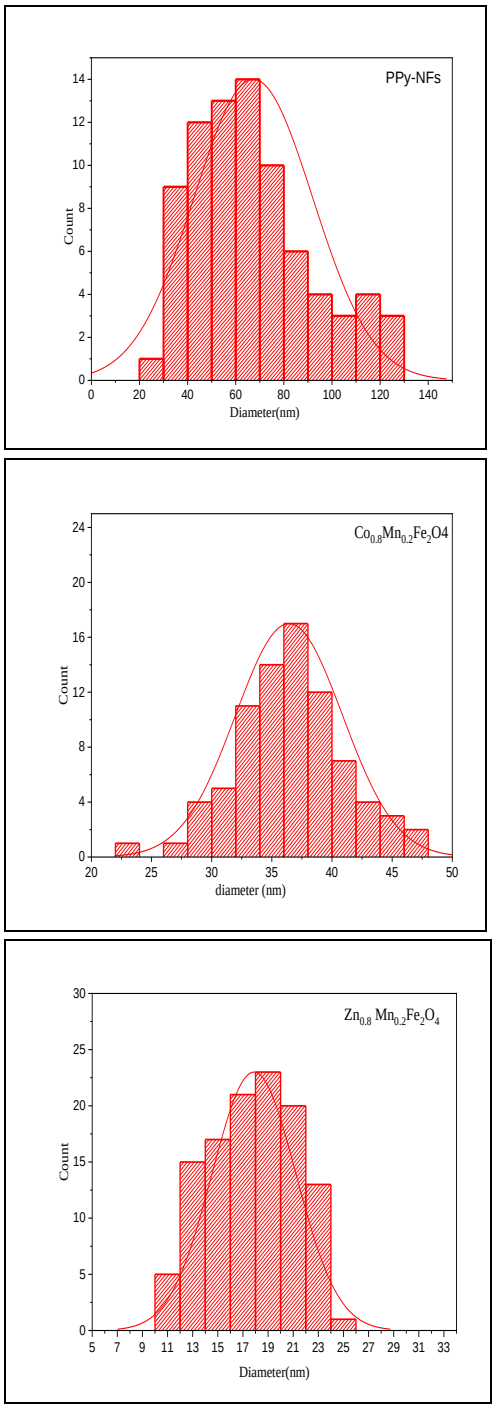

Figure 8. Histograms showing the diameter distribution of PPy-NFs, $Co_{0.8}Mn_{0.2}Fe_2O_4$ and $Zn_{0.8}Mn_{0.2}Fe_2O_4$ nanoparticles.

Magnetic Properties

Figure 9 shows the magnetization of polypyrrole nanofibers (PPy-NFs), nanoferrite and PPy-NFs nanocomposites samples at 300 kelvin with an applied magnetic field from (H) from –10 to +10 kOe. It can be seen that the magnetic properties of PPy-NFs depend on the oxidant concentration (Iron (III) chloride). The retentivity (M_r) of PPy-NFs is 0.58 emu/g and the corresponding coercivity (H_c)

is 74.54 Oe with the maximum magnetization (M_s) of 14.95 emu/g at 10 KOe. There is no doubt that there is a relationship between the magnetization of materials and their internal atomic structure during polymerization process in the presence of the impurity material ($FeCl_3$). Therefore, the origin of magnetization in the (PPy-NFs) polymer returns to the interactions between the non-magnetic PPy-NFs chains and Fe^{+3} ions(Hasan, Bakr, & Ibrahim, 2021; Wang et al., 2009).

The M-H curves of $Co_{0.8}Mn_{0.2}Fe_2O_4$ and $Zn_{0.8}Mn_{0.2}Fe_2O_4$ nanoparticles showed a saturation magnetization (M_s), coercivity (H_c) and retentivity (M_r). As Neel reported that the entire magnetic moments depend on the cations distribution between tetrahedral and octahedral sites in spinel structure (Smart, 1955). From the M-H curves had determined the values of (M_s), (H_c) and (M_r) of $Co_{0.8}Mn_{0.2}Fe_2O_4$ and $Zn_{0.8}Mn_{0.2}Fe_2O_4$ nanoparticles which were 41.15 emu/g, 13.25 Oe, 0.45 emu/g, 10.13emu/g, 35.07 Oe and 0.22 emu/g respectively. From M-H and its derivative curves, there was a clear influence of chemical composition on magnetic behavior. In this investigation, the value of saturation magnetization (M_s) declines as Zinc substitution increases. The decrease in M_s Value with increased nonmagnetic Zn^{2+} ions could be due to the variance in cation distribution between A and B-sites, which reduces the net magnetic moment in the spinel structure. With increasing Cobalt ions content, saturation magnetization increases from 10.13 emu/g to 41.15. This could be because Co^{2+} ions are doped at interstitial sites instead of occupying Fe^{3+} sites in the structure lattice, causing the A-B site's super exchange interaction to be enhanced, resulting in an increase in total magnetic moment. The magnetic Co^{2+} ions dissolve in the spinel lattice, and as the number of magnetic ions grow, the net value of magnetic moment increases. Because of the difference in magnetic moments of Fe^{3+} (5μB) and Co^{2+} (3μB), the magnetic moment of the A-site sublattice (M_A) decreases and the magnetic moment of the B-site sublattice (M_B) increases when Fe^{3+} ions at B-sites are replaced by magnetic Co^{2+} ions. As a result, the value of the net magnetic moment M, which equals M_B-M_A(Anwar & Maqsood, 2014; Chen, Liang, Xiao, & Wei, 2016), will increase.

The magnetic effect was notable in the PPy-NFs nanocomposite samples. The saturation magnetization and retentivity of the composite samples was lower than pure ferrite particles. Almost we noticed Ms, Mr and Hc decrease with decrease of magnetic nanoparticles in the samples that depends mainly on the volume fraction of the magnetic ferrite particles. Furthermore, PPy-NFs contributed to the isolation of magnetic particles and the transformation of ferrite's collinear ferromagnetic order into a noncollinear arrangement, causing ferromagnetic order disruption. Moreover, there may be the surface spin pinning of magnetic moments at ferrite nano particle/support interface, (Sun, Su, Forsling, & Samskog, 1998)which leads to a decrease in magnetic surface anisotropy of ferrite particles. Consequently, the PPy-NFs/ferrite nanocomposites present mostly lower values of coercivity compared with pure ferrite samples (Elahi et al., 2015). We conclude from the foregoing, doping type volume fraction, Grain growth, amount of oxidant, bulk density, anisotropy, and surface are all factors that can alter magnetic characteristics.

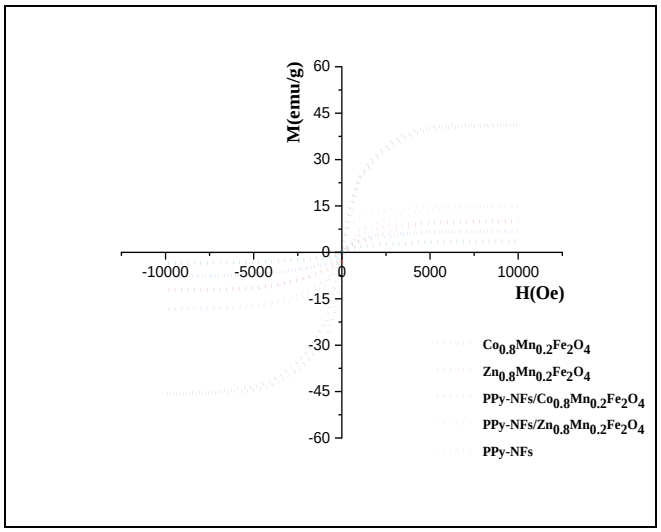

Figure 9. M (emu/g) versus H (Oe) of PPy-NFs, $Co_{0.8}Mn_{0.2}Fe_2O_4$, $Zn_{0.8}Mn_{0.2}Fe_2O_4$ and PPy-NFs nanocomposite samples at 300K

Table 4. Maximum magnetization, remanent magnetization and coercivity at 10 kOe

The samples	M_s ($emug^{-1}$)	M_r ($emug^{-1}$)	H_c (Oe)
$Co_{0.8}Mn_{0.2}Fe_2O_4$	41.15	0.45	13.25
$Zn_{0.8}Mn_{0.2}Fe_2O_4$	10.13	0.22	35.07
PPy-NFs	14.95	0.58	74.54
PPy-NFs/$Co_{0.8}Mn_{0.2}Fe_2O_4$	6.87	0.2	27.5
PPy-NFs/$Zn_{0.8}Mn_{0.2}Fe_2O_4$	3.54	0.16	13.15

Conclusions

Polypyrrole nanofibers, Nanoferrites and polymeric-magneto nanocomposite structures have been synthesized successfully by chemical

polymerization, Heat treatment in a hydrothermal autoclave reactor follows the co-precipitation method and Solution Mixing respectively. The XRD and FESEM results were both consistent and harmony with each other. The magnetic hysteresis loop has been used to calculate M_s, M_r, and H_c. Substitution of Co^{+2} ions increase in the pure ferrite samples which lead to higher magnetization values. Nanoferrite content influences on the magnetic characteristics of nanocomposites as well.

References

Abbas, T., Khan, Y., Ahmad, M., & Anwar, S. (1992). X-ray diffraction study of the cation distribution in the Mn-Zn-ferrites. *Solid state communications, 82*(9), 701-703.

Ahuja, T., & Kumar, D. (2009). Recent progress in the development of nano-structured conducting polymers/ nanocomposites for sensor applications. *Sensors and Actuators B: Chemical, 136*(1), 275-286.

Anwar, H., & Maqsood, A. (2014). Comparison of structural and electrical properties of Co2+ doped Mn-Zn soft nano ferrites prepared via coprecipitation and hydrothermal methods. *Materials Research Bulletin, 49*, 426-433.

Birsöz, B., Baykal, A., Sözeri, H., & Toprak, M. S. (2010). Synthesis and characterization of polypyrrole–$BaFe_{12}O_{19}$ nanocomposite. *Journal of Alloys and Compounds, 493*(1-2), 481-485.

Cabrera, L., Gutierrez, S., Morales, M., Menendez, N., & Herrasti, P. (2009). Magnetic conducting composites based on polypyrrol and iron oxide nanoparticles synthesized via electrochemistry. *Journal of magnetism and magnetic materials, 321*(14), 2115-2120.

Cheah, K., Forsyth, M., & Truong, V.-T. (1998). Ordering and stability in conducting polypyrrole. *Synthetic metals, 94*(2), 215-219.

Chen, D., Liang, Z., Xiao, J.K., & Wei, F.H. (2016). Synthesis of Co-substituted Mn-Zn ferrite nanoparticles by mechanochemistry approach. *Journal of Electroceramics, 36*(1), 158-164.

Choi, M., & Jang, J. (2008). Heavy metal ion adsorption onto polypyrrole-impregnated porous carbon. *Journal of colloid and interface science, 325*(1), 287-289.

Cullity, B. D. (1956). *Elements of X-ray Diffraction*: Addison-Wesley Publishing.

De, A., Sen, P., Poddar, A., & Das, A. (2009). Synthesis, characterization, electrical transport and magnetic properties of PEDOT–DBSA–Fe_3O_4 conducting nanocomposite. *Synthetic metals, 159*(11), 1002-1007.

Elahi, A., Niaz, N., Awan, M., Shakoor, A., Mahmood, K., & Khan, Y. (2015). Structural, electrical, and magnetic properties of polypyrrole–$Zn_{0.5}Ni_{0.45}Mn_{0.05}Fe_2O_4$ nanocomposites prepared by in situ chemical polymerization. *Polymer Science Series B, 57*(6), 738-749.

Ghazanfar, U., Siddiqi, S., & Abbas, G. (2005). Structural analysis of the Mn–Zn ferrites using XRD technique. *Materials Science and Engineering: B, 118*(1-3), 84-86.

Hasan, M.I., Bakr, N.A., & Ibrahim, I.M. (2021). Morphological, magnetic, optical, surface potential, and H_2S gas sensing behavior of polypyrrole nanofibers. *Journal of Electronic Materials, 50*(5), 2716-2724.

Kumar, L., Kumar, P., Narayan, A., & Kar, M. (2013). Rietveld analysis of XRD patterns of different sizes of nanocrystalline cobalt ferrite. *International Nano Letters, 3*(1), 1-12.

MA, C., SG, P., PR, G., Shashwati, S., & VB, P. (2011). Synthesis and characterization of polypyrrole (PPy) thin films. *Soft nanoscience letters, 2011*.

Naseri, M.G., & Saion, E.B. (2012). Crystalization in spinel ferrite nanoparticles. *Advances in crystallization processes*, 349-380.

Ong, C.K., Ray, S., Cooney, R.P., Edmonds, N.R., & Easteal, A.J. (2008). Preparation and characterization of composites of polyethylene with polypyrrole-coated wollastonite. *Journal of applied polymer science, 110*(1), 632-640.

Ouyang, J., & Li, Y. (1997). Great improvement of polypyrrole films prepared electrochemically from aqueous solutions by adding nonaphenol polyethyleneoxy (10) ether. *Polymer, 38*(15), 3997-3999.

Reddy, K.R., Lee, K.P., Lee, Y., & Gopalan, A.I. (2008). Facile synthesis of conducting polymer–metal hybrid nanocomposite by in situ chemical oxidative polymerization with negatively charged metal nanoparticles. *Materials Letters, 62*(12-13), 1815-1818.

Sanches, E.A., Alves, S.F., Soares, J.C., Da Silva, A.M., Da Silva, C.G., De Souza, S.M., & Da Frota, H.O. (2015). Nanostructured polypyrrole powder: a structural and morphological characterization. *Journal of Nanomaterials, 2015*.

Smart, J.S. (1955). The Néel theory of ferrimagnetism. *American Journal of Physics, 23*(6), 356-370.

Smith, J., & Wijn, H. (1959). Ferrites: physical properties of ferromagnetic oxides in relation to their technical applications. *Phillips Technical Library, Eindhoven*.

Sun, Z.X., Su, F.W., Forsling, W., & Samskog, P.O. (1998). Surface characteristics of magnetite in aqueous suspension. *Journal of colloid and interface science, 197*(1), 151-159.

Syue, M.R., Wei, F.J., Chou, C.S., & Fu, C.M. (2011). Magnetic, dielectric, and complex impedance properties of nanocrystalline Mn–Zn ferrites prepared by novel combustion method. *Thin Solid Films, 519*(23), 8303-8306.

Truong, V.T., Riddell, S., & Muscat, R. (1998). Polypyrrole based microwave absorbers. *Journal of materials science, 33*(20), 4971-4976.

Wang, X., Tang, S., Liu, J., He, Z., An, L., Zhang, C., Feng, W. (2009). Uniform Fe_3O_4–PANi/PS composite spheres with conductive and magnetic properties and their hollow spheres. *Journal of Nanoparticle Research, 11*(4), 923-929.

Zhang, C., Li, Q., & Ye, Y. (2009). Preparation and characterization of polypyrrole/nano-$SrFe_{12}O_{19}$ composites by in situ polymerization method. *Synthetic metals, 159*(11), 1008-1013.